Linear and Quadratic Optimal Power Flow Models of a Hybrid Network based on VSC-MTDC

Journal:	*IEEE Transactions on Power Systems*
Manuscript ID	TPWRS-00104-2016
Manuscript Type:	Transactions
Date Submitted by the Author:	18-Jan-2016
Complete List of Authors:	Zhao, Quanyu; Institute for Research in Technology, ICAI School of Engineering, Comillas Pontificia Universidad García-González, Javier; Universidad Pontificia Comillas, Instituto de Investigación Tecnológica (IIT)
Technical Topic Area :	Power system operations, Power system expansion planning
Key Words:	Optimal Power Flow, Multi-Terminal HVDC, AC/DC Transmission System, Piecewise linear approximation, Cost Minimization

SCHOLARONE™
Manuscripts

Linear and Quadratic Optimal Power Flow Models of a Hybrid Network based on VSC-MTDC

Quanyu Zhao, *Student Member, IEEE,* Javier García-González, *Member, IEEE,*

***Abstract*—Optimal Power Flow (OPF) models are essential tools not only from the daily operational point of view, but also for medium-term and long term studies. In this case, when it is necessary to consider future expansion planning, the size of the resulting problem can be intractable. This paper presents two approximated (linear and quadratic) formulations of the OPF considering a combination of a Voltage Source Converter based Multi-Terminal High Voltage Direct Current grid (VSC-MTDC) and an alternating current (AC) system. The models presented in the paper take into account both transmission losses and converter losses. The key technical limits of VSC are included in both models as constraints for VSC-MTDC system operation. All the study results are verified and compared with the full power flow solver based on MATPOWER. The models allow to obtain good approximations of power flows and voltage levels of all DC buses within a reasonable range of accuracy, as well as to model the interaction between AC and DC networks with a substantial lower computational burden compared with the state-of-the-art non-linear OPF models.**

***Index Terms*—Optimal Power Flow, Multi-Terminal HVDC, AC/DC Transmission System, Piecewise Linear, Cost Minimization**

NOMENCLATURE

Upper-case letters are used for denoting parameters and sets. Lower-case letters denote variables and indexes. Real power is expressed in [MW], reactive power in [MVAr], and complex power in [MVA]. The symbols "~" and "−" above characters are used to denote AC and DC variables respectively.

A. Indexes, sets and subsets

$g \in \mathcal{G}$	Generating units, running from 1 to G.
$i, j \in \mathcal{B}$	Buses, running from 1 to B.
$l \in \mathcal{L}$	Transmission lines, running from 1 to L.
$v \in \mathcal{V}$	VSC converter, running from 1 to V.
$(i,j) \in \mathcal{N}_l$	Pair of buses connected by line l.
$\tilde{\mathcal{L}} \subset \mathcal{L}$	Subset of AC transmission lines.
$\bar{\mathcal{L}} \subset \mathcal{L}$	Subset of DC transmission lines.
$\tilde{\mathcal{B}} \subset \mathcal{B}$	Subset of AC buses.
$\bar{\mathcal{B}} \subset \mathcal{B}$	Subset of DC buses.
$\tilde{\mathcal{N}}_v$	AC bus of converter v.
$\bar{\mathcal{N}}_v$	DC bus of converter v.

B. Parameters

x_l	Reactance of line l [p.u.].
r_l	Resistance of line l [p.u.].
g_l	Conductance of line l [p.u.].
b_l	Susceptance of line l [p.u.].
b_l^{sht}	Half total line charging susceptance of line l [p.u.].
b_f	Filter susceptance [p.u.].
a_g,b_g,c_g	Cost coefficients of generator g.
c_p,c_q	Costs of non-served real and reactive power.
a_v,b_v,c_v^{rec},c_v^{inv}	Loss coefficients of converter v.
$\overline{S}_l$,$\underline{S}_l$	Flow limits on transmission line l.
$\overline{I}_v$,$\underline{I}_v$	Phase current limits on converter v.
$\overline{P}_g$,$\underline{P}_g$	Real power limits of generator g.
$\overline{Q}_g$,$\underline{Q}_g$	Reactive power limits of generator g.
$\overline{V}_i$,$\underline{V}_i$	Voltage limits at bus i.
P_{Di},Q_{Di}	Real and reactive power demand at bus i.
$\mathbf{Y}^{\mathrm{ac}}$	AC network admittance matrix [p.u.]
$\mathbf{Y}^{\mathrm{dc}}$	DC network admittance matrix [p.u.]
$\mathbf{G}$	AC network conductance matrix [p.u.]
$\mathbf{B}$	AC network susceptance matrix [p.u.]
S_B	Base power [MVA].

C. Decision Variables

p_i,q_i	Real and reactive power injected at bus i.
ρ_v,ρ_l	Active losses of converter v and line l.
np_i,nq_i	Non-served Real and reactive power at bus i.
v_i,θ_i	Voltage magnitude and phase angle at bus i [p.u.], [rad].
p_g,q_g	Real and reactive power generation of generator g.
i_v	Phase current of converter v [p.u.].

I. INTRODUCTION

MEETING the rising energy requirements in a sustainable, secure and competitive manner is one of the main challenges of current power systems. In this context, the development of a 'Supergrid' has been proposed as a promising solution to harness geographically dispersed low-carbon energy sources (such as offshore wind and solar), and also to facilitate the cross-border trading and the integration of wholesale electricity markets [1]. For instance, in the European system, 150 GW of total installed offshore capacity of wind energy producing 562 TWh of electricity is expected by 2030 [2], and increasing the capacity of the transnational interconnections is in the agenda of the current EU energy policy [3].

Despite the existence of many barriers such as the cost of converter stations, less standardized equipment as compared

Quanyu Zhao and Javier García-González are with the Institute of Technological Research (IIT), ICAI School of Engineering, Comillas Pontifical University, Madrid, Spain e-mail: quanyu.zhao@comillas.edu, javiergg@comillas.edu.

with AC systems, need of new control algorithms, difficulty to build DC breakers, etc., High Voltage Direct Current (HVDC) systems with Multi-Terminal (MTDC) configuration are seen as a viable option that can outperform traditional AC transmission due to its technical, economic and environmental advantages.

The impact on power flows derived from point-to-point (PTP) interconnections between HVAC and HVDC systems is even more notable in case of having a meshed MTDC system overlaying an AC grid, and the control strategies of the converters become crucial. Voltage Source Converter (VSC) allows flexible and independent active and reactive power control [5], and its forced-commuted feature makes it ideal to connect wind farms at distance as it can mitigate the propagation of voltage and frequency deviations caused by wind variations. However, the operating principles of VSC are completely different from those of current source converter (CSC). Therefore, new algorithms have been developed for VSC HVDC control and power flow studies.

The problem of finding the power flow solution for the case of hybrid network with VSC-MTDC systems is relatively new [4], [8]. Among the few papers that study the power flow (PF) problem of a hybrid network in the literature, it is possible to distinguish basically between: 1) the sequential approach as in [6] where AC and DC systems are solved separately under a general formulation that can deal with converter limits and different topologies; and 2) the unified approach as in [7] where AC and DC systems are solved together with an explicit consideration of converter losses that are balanced with a DC slack bus per MTDC grid in the system. Some other authors have been focusing on the transient analysis and stability issues, which is out of the scope of this paper.

In addition to the power flow problem, the optimal power flow (OPF) was firstly introduced by Carpentier in 1962 [15]. The goal is to find the optimal scheduling of the generators while taking into account network constraints (capacity limits and security constraints). In order to assess and fully exploit the potential impact of VSC-MTDC, traditional models that were developed for AC systems need to be extended to cope with hybrid AC-DC networks. Several research works have been proposed to include VSC-MTDC system into power flow calculation of a hybrid AC-DC system as previously mentioned. However, fewer studies take into account VSC-MTDC systems under an optimization context: [8] applies Second-Order Cone Programming (SOCP) technique, [18] solves the hybrid network using the Primal-Dual Interior Point (PDIP) algorithm, with predefined control strategies for DC networks, as well as modified Jacobian and Hessian matrices, and [9] utilizes Interior Point Optimizer (IPOPT) to seek solutions for the non-linear model built in General Algebraic Modeling System (GAMS).

OPF models are not only used for short-term system operations. They can also serve as sub-modules to assist long-term expansion planning problems [22]. The economic assessment of considering VSC-MTDC systems as an alternative for network reinforcement instead of conventional AC links becomes one of the most important tasks during the overall planning stage. To the authors' knowledge, [9] is the only work that copes with such a problem. Thus, the main objective of this paper is to propose extended OPF tools for AC networks integrated with embedded VSC-MTDC systems of diverse topologies, which could be applied for both operation and planning purposes.

The major contributions of this paper is the development of two simplified, steady-state OPF models that are able to cope with hybrid AC-DC networks, taking into account both transmission and converter limits and losses:

• Among all relevant literature reviewed, there are no previous works in which OPF models for hybrid networks are able to solve large scale problems. The two models proposed in this paper can deal with big systems with a good level of accuracy since they are formulated as linear or as quadratic programming optimization models.

• A detailed representation of the converters and transmission losses are included in both models. In particular, they are capable of capturing the different reported performance of the converters when functioning either as inverters or rectifiers.

• The state-of-the-art non-linear model presented in [9] has been improved for the purpose of replicating the case study from MATACDC. In this way, it can be used as benchmark to compare the goodness of the solution obtained with the simplified models, and to analyze their performance in terms of computational burden.

This paper is organized as follows. In Section II, equations used for modeling a hybrid network are presented. Section III provides the detailed formulation of the presented models and Section IV presents their validation. The results and discussions of the case study are presented in Section V. Finally, conclusions are drawn in Section VI.

II. Equations of a Hybrid AC-DC Network

A. AC-grid power flow equations

Every bus i of the AC grid is characterized by its voltage magnitude v_i and phase angle θ_i. Every line l connecting a pair of AC buses can be represented by its series resistance r_l and reactance x_l. Assuming that the line charging susceptance can be represented by assigning half of its value to the extreme nodes of the line, b_l, it is possible to build the AC network admittance matrix $\mathbf{Y}^{ac}$ with real and imaginary matrices $\mathbf{G}$ and $\mathbf{B}$ respectively [15]. The diagonal terms (Y_{ii}^{ac}denoted as "self admittance"), are the sum of the admittances of all devices incident to bus i. The off-diagonal terms, Y_{ij}^{ac}, are equal to the negative of the admittance joining the two buses.

$$\mathbf{Y}^{ac} = \mathbf{G} + j\mathbf{B} \tag{1}$$

By denoting $\theta_{ij} = \theta_i - \theta_j$, power injections at node i are [15]:

$$p_i = S_B \cdot v_i \sum_{j \in \mathcal{B}_{\text{ac}}} v_j \left[G_{ij} cos\left(\theta_{ij}\right) + B_{ij} sin\left(\theta_{ij}\right) \right] \tag{2}$$

$$q_i = S_B \cdot v_i \sum_{j \in \mathcal{B}_{\text{ac}}} v_j \left[G_{ij} sin\left(\theta_{ij}\right) - B_{ij} cos\left(\theta_{ij}\right) \right] \tag{3}$$

B. DC-grid power flow equations

Every bus i of the DC grid is characterized by its voltage magnitude v_i. Every line l connecting a pair of DC buses can be represented by its resistance r_l. Assuming that the extreme nodes of such line are i and j, the element (i, j) of the DC admittance matrix (which contains pure conductances in DC networks) $\mathbf{Y}^{dc}$can be defined as:

$$Y_{ij}^{dc} = \frac{1}{r_l} \tag{4}$$

The real power injected at node i of the DC grid satisfy the following expression, where it is assumed a symmetric monopolar configuration:

$$p_i = 2 \cdot S_B \cdot v_i \sum_{j \in \mathcal{B}_{\text{dc}}} Y_{ij}^{dc} \left(v_i - v_j\right) \tag{5}$$

C. VSC converter station model

The VSC converter station comprises all the elements that connect the AC and the DC networks (see Fig. 1). At the converter, the voltage waveform is synthesized either by Pulse Width Modulation (PWM) that requires low pass filters to block the flow of higher order harmonics, or by a Multi-modular Converter approach (MMC). Finally, the filter bus is connected to the AC network through a transformer. Power can be injected on both sides, depending on the flow direction variables, $\tilde{p}_v, \tilde{q}_v$ and $\bar{p}_v$ can be either positive or negative. However, converter losses ρ_v cannot be negative.

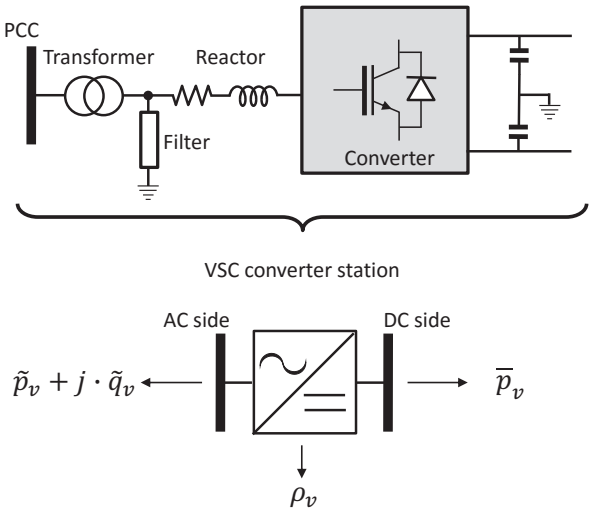


Figure 1. Schematics of the VSC-Converter Station

As described in [6][9], the most common approach is to represent the VSC converter as a controllable voltage source $\underline{v}_c = v_c \angle \theta_c$ connected by a phase reactor $\underline{z}_c = r_c + jx_c$ to an intermediate node where a lossless shunt filter is connected ($\underline{z}_f = -j/b_f$). The voltage at this intermediate node is $v_f \angle \theta_f$, and the transformer that be represented by its impedance: $\underline{z}_{tf} = r_{tf} + jx_{tf}$ (see Fig. 2).

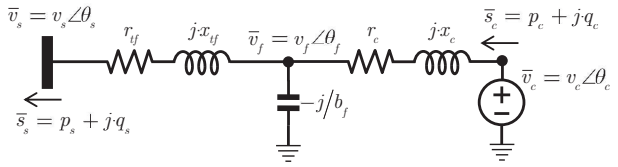


Figure 2. Equivalent circuit of the VSC-Converter Station

It is important to notice that for each VSC converter station, two more AC buses are added to the system: the filter bus, and the converter bus. In case of not being necessary to install the filter (or when its effect can be neglected), both the phase reactor and the transformer impedance can be lumped together, eliminating from the equations the corresponding voltage magnitude and phase angle of the filter bus. As a consequence, the power flow within the VSC converter station between the nodes c, f, and s have to comply with (2) and (3). In that case, the shunt susceptance only affect the diagonal terms of the matrix $\mathbf{B}$ at the position of the filter buses. Depending on the level of accuracy (transformer- or filter-less), converter power injection to the AC network $\tilde{p}_v + j\tilde{q}_v$ can be treated equivalent as $\bar{S}_c = p_c + jq_c$ or $\bar{S}_s = p_s + jq_s$.

There are mainly three factors limiting the operation of a VSC HVDC system [18]:

• *Maximum current through the IGBTs.*

• *DC voltage level.* This limit couples the voltage level of the converters on both sides [21]. In this paper, the factor k_v is set to be 1.1:

$$v_c \leq k_v \cdot v_i \qquad \forall v \in \mathcal{V}, c \in \tilde{\mathcal{N}}_v, i \in \tilde{\mathcal{N}}_v, \tag{6}$$

• *Maximum current through the DC cables* which is equivalent to setting the maximum DC power transfer as (34).

Previous imposed limits have further derived boundaries on active and reactive power injected to the AC network [6][9]:

$$p_v^2 + q_v^2 = \left(v_c \cdot i_v\right)^2 \qquad \forall c \in \tilde{\mathcal{N}}_v, v \in \mathcal{V} \tag{7}$$

In addition, as explained in [20], there can exist a minimum reactive power of -0.5 p.u. imposed to the converters as in [9]:

$$q_v \geq \underline{q_v} = -\frac{\overline{Q}_v}{2} \qquad \forall v \in \mathcal{V} \tag{8}$$

Apart from the limits aforementioned, converters can be subject to certain requirement from the Grid Codes. For example, in [18], the converters are obliged to have a reactive power capacity of 0.95 power factor lagging to 0.95 leading at the connection point.

Furthermore, although in [9] all converter losses are assigned to the AC side, in this paper, they are assumed to be on the DC side as in [6] in order to replicate the very same criterion used in the validation tool MATACDC.

D. Network and Converter Losses

Denoting transmission losses of line l connecting nodes i and j by ρ_l, its expression for AC lines can be written as follows [15]:

$$\rho_l = S_B \cdot \left\{ g_l \left[v_i^2 + v_j^2 - 2 \cdot v_i v_j cos\left(\theta_{ij}\right) \right] \right\} \ \forall l \in \tilde{\mathcal{L}}, (i,j) \in \mathcal{N}_l \tag{9}$$

Similarly, for DC lines:

$$\rho_l = S_B \cdot \left(r_l \cdot i_{ij}^2 \right) \qquad \forall l \in \bar{\mathcal{L}}, (i,j) \in \mathcal{N}_l \tag{10}$$

The converter station losses are also taken into account in the models developed in this paper using a generalized quadratic expression that depends on the VSC phase current [6]:

$$\rho_v = a_v + b_v \cdot |i_v| + c_v^{inv} \cdot i_v^{+2} + c_v^{rec} \cdot i_v^{-2} \tag{11}$$

where $i_v = i_v^+ - i_v^-$ and $i_v^+,\ i_v^- \geqslant 0$, which implies $|i_v| = i_v^+ + i_v^-$. Depending on the phase current direction, the VSC can either function as a rectifier or a inverter corresponding to different c values. As exemplified in (11), either $c_v^{inv} \cdot i_v^{+2}$ or $c_v^{rec} \cdot i_v^{-2}$ will be zero. This feature has also been taken into consideration in the models proposed in the paper.

E. Objective Function

The considered objective function is to minimize the total operating costs plus the penalty from the non-served active and reactive power as shown in (12). There are some other alternatives, such as minimization of network losses as in [18], which could also be easily adapted.

III. Mathematical Formulation

In this section, detailed mathematical formulations are presented for the three models respectively. For simplicity, all variables presented in this section are in [p.u.], and units of corresponding parameters are adapted accordingly.

*A. Non Linear Programming OPF Model (**NLP-OPF**)*

The non-linear model presented in this paper is built based on the groundwork of [9], which has been improved to include converter loss dependency on the phase current direction, i.e., functioning either as a inverter or a rectifier.

$$\min \sum_{g \in \mathcal{G}} \left(c_g + a_g \cdot p_g + b_g \cdot p_g^2 \right) + \sum_{i \in \mathcal{B}} \left(c_p \cdot np_i + c_q \cdot nq_i \right) \tag{12}$$

s.t.

$$p_i = v_i \sum_{j \in \tilde{\mathcal{B}}} v_j \left[G_{ij} cos\left(\theta_{ij}\right) + B_{ij} sin\left(\theta_{ij}\right) \right], \forall i \in \tilde{\mathcal{B}} \tag{13}$$

$$p_l = v_i^2 g_l - v_i v_j \left[g_l cos\left(\theta_{ij}\right) + b_l sin\left(\theta_{ij}\right) \right], \quad \forall l \in \tilde{\mathcal{L}},\ (i,j) \in \mathcal{N}_l \tag{14}$$

$$q_i = v_i \sum_{j \in \tilde{\mathcal{B}}} v_j \left[G_{ij} sin\left(\theta_{ij}\right) - B_{ij} cos\left(\theta_{ij}\right) \right], \forall i \in \tilde{\mathcal{B}} \tag{15}$$

$$q_l = -v_i^2 \left(b_l + b_l^{sht} \right) - v_i v_j \left[g_l cos\left(\theta_{ij}\right) - b_l sin\left(\theta_{ij}\right) \right], \quad \forall l \in \tilde{\mathcal{L}},\ (i,j) \in \mathcal{N}_l \tag{16}$$

$$p_i = 2 \cdot v_i \sum_{j \in \bar{\mathcal{B}}} G_{ij} \left(v_i - v_j \right), \forall i \in \bar{\mathcal{B}} \tag{17}$$

$$p_l = 2 \left[v_i \left(v_i - v_j \right) / r_l \right], \forall l \in \bar{\mathcal{L}},\ (i,j) \in \mathcal{N}_l \tag{18}$$

$$p_i = \sum_{g \in \mathcal{G}_i} \left(p_g \right) - P_{Di} + \sum_{v \in \mathcal{V}_i} \tilde{p}_v + np_i, \forall i \in \tilde{\mathcal{B}} \tag{19}$$

$$p_i = \sum_{v \in \mathcal{V}_i} \left(\bar{p}_v + \rho_v \right) + np_i, \forall i \in \bar{\mathcal{B}} \tag{20}$$

$$q_i = \sum_{g \in \mathcal{G}_i} \left(q_g \right) - Q_{Di} + \sum_{v \in \mathcal{V}_i} q_v + nq_i, \forall i \in \tilde{\mathcal{B}} \tag{21}$$

$$0 = \left(i_v v_c \right)^2 - \left(\tilde{p}_v^2 + q_v^2 \right), \forall v \in \mathcal{V},\ c \in \tilde{\mathcal{N}}_v \tag{22}$$

$$0 \leq i_v \cdot \tilde{p}_v, \forall v \in \mathcal{V} \tag{23}$$

$$0 = \bar{p}_v + \tilde{p}_v + \rho_v, \forall v \in \mathcal{V} \tag{24}$$

$$i_v = i_v^+ - i_v^-; i_v^+ \geq 0; i_v^- \geq 0, \forall v \in \mathcal{V} \tag{25}$$

$$\rho_v = a_v + b_v \left(i_v^+ + i_v^- \right) + c_{inv} i_v^{+2} + c_{rec} i_v^{-2}, \forall v \in \mathcal{V} \tag{26}$$

$$\underline{I}_v \leq i_v \leq \overline{I}_v, \forall v \in \mathcal{V} \tag{27}$$

$$v_c \leq k_v \cdot v_i, \forall v \in \mathcal{V}, c \in \tilde{\mathcal{N}}_v, i \in \bar{\mathcal{N}}_v \tag{28}$$

$$q_v \geq \underline{q_v}, \forall v \in \mathcal{V} \tag{29}$$

$$\underline{V}_i \leq v_i \leq \overline{V}_i, \forall i \in \mathcal{B} \tag{30}$$

$$\underline{P}_g \leq p_g \leq \overline{P}_g, \forall g \in \mathcal{G} \tag{31}$$

$$\underline{Q}_g \leq q_g \leq \overline{Q}_g, \forall g \in \mathcal{G} \tag{32}$$

$$\overline{S}_l^2 \geq p_l^2 + q_l^2, \forall l \in \tilde{\mathcal{L}} \tag{33}$$

$$\overline{P}_l^2 \geq p_l^2, \forall l \in \bar{\mathcal{L}} \tag{34}$$

$$np_i \geq 0, nq_i \geq 0, \forall i \in \mathcal{B} \tag{35}$$

Nodal balance equations (13), (15) and (17) are (2), (3) and (5) expressed in [p.u.] respectively, from which, power flow equations (14), (16) and (18) can be easily derived. Conservation of power seen from AC and DC sides respectively are established through (19) and (20). (19) establishes that the total active power injected in every AC node must be equal to the sum of all the local generation, minus the demand in that node, plus the active power injected by the converter (in case there is one), and plus the non-served active power. (21) follows a similar expression as (19) for the case of reactive power. Likewise, a power balance equation is established in (20) to the DC grid, where it has been assumed that there are no generators or consumers connected to directly. In case of being necessary to consider the opposite case, equation (20) could be modified straightforwardly. (22) is the same as (7). The direction of phase current is identified through constraint (23) to differentiate converters as inverters or rectifiers. Power balance within the converter is established by (24) as illustrated in Fig. 1. (25) and (26) together provide the complete converter modeling. Equation (27) - (35) establish a set of common technical limits for AC and DC bus voltage, generator active and reactive power, as well as AC and DC transmission line flows.

*B. Quadratic Programming OPF Model (**QCP-OPF**)*

In the quadratic simplified formulation, trigonometric functions can be simplified as $\cos(x) \backsimeq 1 - \frac{x^2}{2}$ and $\sin(x) \backsimeq x$. In addition, AC voltage levels are omitted in power flow equations of AC network assuming nominal values, i.e., 1 in p.u.

$$\min \sum_{g\in\mathcal{G}} \left(c_g + a_g \cdot p_g + b_g \cdot p_g^2\right) + \sum_{i\in\mathcal{B}} \left(c_p \cdot np_i\right) \quad (36)$$

s.t.

$$p_i = \sum_{j\in\tilde{\mathcal{B}}} \left[G_{ij}(1-\theta_{ij}^2/2) + B_{ij}\theta_{ij}\right], \forall i \in \tilde{\mathcal{B}} \quad (37)$$

$$p_l = g_l - \left[g_l\left(1-\theta_{ij}^2/2\right) + b_l\theta_{ij}\right], \quad \forall l \in \tilde{\mathcal{L}},\ (i,j) \in \mathcal{N}_l \quad (38)$$

$$p_i = 2 \cdot v_i \sum_{j\in\bar{\mathcal{B}}} G_{ij}\left(v_i - v_j\right), \forall i \in \bar{\mathcal{B}} \quad (39)$$

$$p_l = 2\left[v_i\left(v_i - v_j\right)/r_l\right], \forall l \in \bar{\mathcal{L}},\ (i,j) \in \mathcal{N}_l \quad (40)$$

$$p_i = \sum_{g\in\mathcal{G}_i} (p_g) - P_{Di} + \sum_{v\in\mathcal{V}_i} \tilde{p}_v + np_i, \forall i \in \tilde{\mathcal{B}} \quad (41)$$

$$p_i = \sum_{v\in\mathcal{V}_i} (\bar{p}_v + \rho_v) + np_i, \forall i \in \bar{\mathcal{B}} \quad (42)$$

$$0 = i_v - \tilde{p}_v, \forall v \in \mathcal{V} \quad (43)$$

Constraints (24) - (31) and (33) - (35) are also included in this model.

Power injected at node i and power flow on line l between node i and j are represented as (37) and (38). Notice that AC transmission losses implicitly taken into account in *QCP-OPF* are $\rho_l \simeq g_l\left(\theta_{ij}\right)^2$ which is coherent with (9) after introducing the mentioned simplification of the trigonometric functions.

C. Linear Programming OPF Model (*LP-OPF*)

This model is built based on the well-known DC-OPF[1] formulation [15], and it has been extended to include HVDC networks and converter modeling. Thus AC voltage magnitudes are assumed to take nominal values.

$$\min \sum_{g\in\mathcal{G}} \left(c_g + a_g \cdot p_g + b_g \cdot p_g^2\right) + \sum_{i\in\mathcal{B}} \left(c_p \cdot np_i\right) \quad (44)$$

s.t.

$$p_i = \sum_{j\in\tilde{\mathcal{B}}} B_{ij}\theta_{ij} + \sum_{(i,j)\in\mathcal{N}_l} \frac{\rho_l}{2}, \forall i \in \tilde{\mathcal{B}} \quad (45)$$

$$p_l = b_l\theta_{ij}, \forall l \in \tilde{\mathcal{L}},\ (i,j) \in \mathcal{N}_l \quad (46)$$

$$\rho_l = f\left(p_l\right) = r_l p_l^2, \forall l \in \tilde{\mathcal{L}} \quad (47)$$

$$p_i = 2\sum_{j\in\bar{\mathcal{B}}} G_{ij}\left(v_i - v_j\right) + \sum_{(i,j)\in\mathcal{N}_l} \frac{\rho_l}{2}, \forall i \in \bar{\mathcal{B}} \quad (48)$$

$$p_l = 2\left[\left(v_i - v_j\right)/r_l\right], \forall l \in \bar{\mathcal{L}},\ (i,j) \in \mathcal{N}_l \quad (49)$$

$$\rho_l = f\left(p_l\right) = r_l p_l^2, \forall l \in \bar{\mathcal{L}} \quad (50)$$

$$p_i = \sum_{g\in\mathcal{G}_i} (p_g) - P_{Di} + \sum_{v\in\mathcal{V}_i} \tilde{p}_v + np_i, \forall i \in \tilde{\mathcal{B}} \quad (51)$$

$$p_i = \sum_{v\in\mathcal{V}_i} (\bar{p}_v + \rho_v) + np_i, \forall i \in \bar{\mathcal{B}} \quad (52)$$

$$0 = i_v - \tilde{p}_c, \forall v \in \mathcal{V},\ c \in \tilde{\mathcal{N}_v} \quad (53)$$

[1]This model proposed is called LP-OPF instead of DC-OPF to avoid confusion, and both AC and DC grids are considered.

Constraints (24) - (31) and (33) - (35) are also included in this model.

Power injected at node i and power flow on line l between node i and j are represented as (45) and (46), where ρ_l represents the losses. These losses can be treated as additional loads at the extreme nodes of the line [17]. From (9), by using the well-known DC load flow approximation, the loss expression can be readily reduced to (47) [19]. Notice that (47) and (50) are not linear expressions. However they can be approximated by a set of linear constraints as the *Model3a* reviewed in [16], which has been left out here for the sake of simplicity. On the other hand, power injected at node i and power flow on line l between node i and j of DC network are represented as (48) and (49), where ρ_l is again approximated with a standard piecewise linear method [16].

IV. Validation

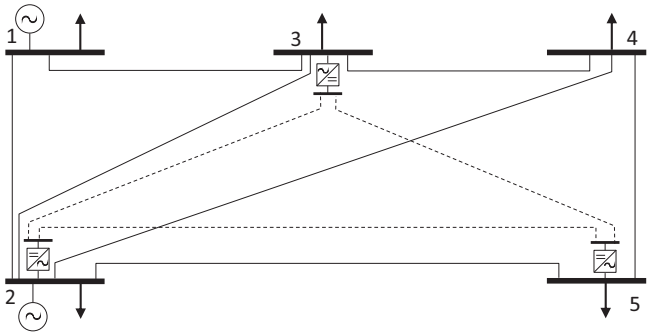


Figure 3. 5-bus Leuven System

In order to validate the models, the test system presented in [12] has been chosen. The authors from [12] have developed a VSC-MTDC power flow solver, i.e., MATACDC, on the basis of MATPOWER. In this paper, the three models presented in Section III have been developed in GAMS [10]. The most complex model (*NLP-OPF*) takes into account all non-linearities and successfully replicates exactly the results produced by MATACDC with IPOPT solver [13]. In addition, power flow results of simplified models are provided below.

Table I
Power Flow [MW] of both AC and DC Branches

Branch	Exact/NLP	LP	QCP
$P_{1AC-2AC}$	98.38	97.57	97.46
$P_{1AC-3AC}$	35.26	34.54	34.87
$P_{2AC-3AC}$	13.25	13.52	13.71
$P_{2AC-4AC}$	17.08	17.29	17.46
$P_{2AC-5AC}$	25.33	25.41	25.24
$P_{3AC-4AC}$	23.09	22.60	22.31
$P_{4AC-5AC}$	−0.07	−0.26	−0.47
$P_{3DC-2DC}$	−30.66	−30.37	−29.99
$P_{3DC-5DC}$	8.52	8.69	8.95
$P_{2DC-5DC}$	27.96	27.83	27.96
$P_{2AC-2DC}$	60.00	60.00	58.98
$P_{3AC-3DC}$	−20.76	−20.21	−19.90
$P_{5AC-5DC}$	−35.00	−35.00	−35.52

Both *LP-OPF* and *QCP-OPF* provide quite precise approximations for almost all lines. Big discrepancy happens on

the nodal injection $P_{3^{DC}}$, which are 0.55MW and 0.86MW for *LP-OPF* and *QCP-OPF* respectively; and on AC line $P_{4^{AC}-5^{AC}}$, which are almost 4 and 7 times the exact value accordingly. For *LP-OPF*, average mismatch of these 13 line flows is 0.06 MW, while the average flow is 30.26 MW, making the error around 0.20%. Without considering flow $P_{4^{AC}-5^{AC}}$, the mean absolute percentage error (MAPE) is 1.22%. On the other hand, *QCP-OPF* also gives a good result in general: average mismatch of 0.10 MW, which makes the error 0.33%. Without considering flow $P_{4^{AC}-5^{AC}}$, the MAPE is 2.18%.

Table II
DC VOLTAGE [P.U.] LEVEL COMPARISON

Bus	Exact/NLP	LP	QCP
$V_{3^{DC}_{(slack)}}$	1.00000	1.00000	1.00000
$V_{2^{DC}}$	1.00791	1.00789	1.00780
$V_{5^{DC}}$	0.99778	0.99774	0.99767

Table II shows a comparison of the DC voltage level within the 3-terminal MTDC network. Bus 3^{DC} is assumed to be the DC slack bus to cover all the losses in DC network. As can be seen from the table, there are very few differences between the complete power flow solutions and the proposed methods. From the results shown above, it can be concluded that both *LP-OPF* and *QCP-OPF* provide good approximations. In order to explore how such models perform in other conditions, a larger system is studied in the next section.

V. CASE STUDY

A. System Description

The study case is the very same system used in [6], including all VSC converter parameters shown in Table III. It is based on a Modified IEEE Two Area RTS-96 (MRTS) network [11]. Fig.4 provides the single line diagram of the MRTS system.

In the MRTS network, interconnection 107-203 is replaced by a 3-terminal MTDC network with an additional offshore wind farm (buses 301 and 302) in between. Lines 113-215 and 123-217 are replaced by a 4-terminal MTDC network. The reference (slack) buses for AC system are at bus 113, 213 and 302 respectively, while VSC_1 and VSC_4 are chosen to be the slack buses for MTDC systems. Two generators, located at bus 107 and 201, are disabled and replaced by the offshore wind farm at bus 302. Different cost coefficients assigned to generators can be found in Table IV [14]. All power injections and voltage levels at VSCs are considered decision variables.

B. Numerical Results

The OPF problem is solved with the three proposed models respectively. Results shown in this paper were generated by using solver CPLEX 12.6 [13] for the *LP-QCP* and *QCP-OPF*, and IPOPT for the *NLP-OPF* model, on an Intel-i7 2.93-GHz personal computer with 4GB of RAM memory. Problems are solved with default values of solver parameters (relative optimality tolerance, maximum number of iterations, etc.). The purpose of the case study is to focus on cross-comparison of the proposed two simplified OPF models, using the non-linear model as a reference.

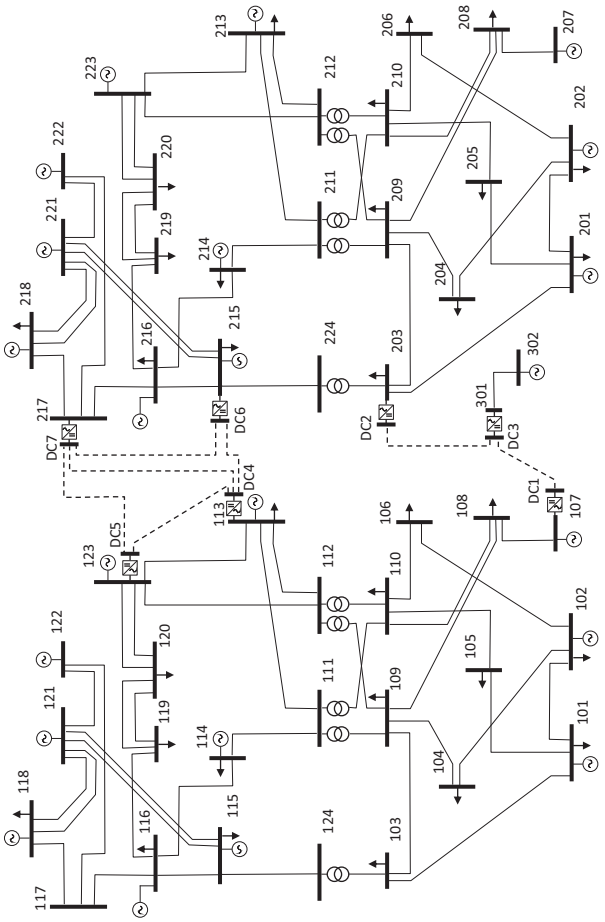


Figure 4. IEEE Two Area RTS-96 with two HVDC networks

Table III
VSC CONVERTER DATA

Converter	Parameters	Rating & Converter Loss Data				
		$No.$	1, 2	3	4, 6	5, 7
$X_{tr}(p.u.)$	0.1121	$P_{dc}(MW)$	100	200	200	100
$R_{tr}(p.u.)$	0.0015	$\pm V_{dc}(kV)$	150	150	300	300
$B_f(p.u.)$	0.0887^a	$a\,(MW)$	1.103	2.206	1.103	2.206
$X_c(p.u.)$	0.16428	$b\,(kV)$	0.887	0.887	1.800	1.800
$R_c(p.u.)$	0.0001	$c_v^{rec}\,(\Omega)$	2.885	1.442	5.94	11.88
		$c_v^{inv}\,(\Omega)$	4.371	2.185	9	18

[a] Only included for converters 4-7

Branch power flows of both AC and DC grids are shown in Table VI and Table VII respectively. Generation levels for all generators are illustrated in Table V.

Generation levels of all generators play a more important role as part of a complete optimal power flow solution. It can be easily observed from the table that, only generators from buses No. 107, 207, 213 and 302 have different outputs, while all others keep the same generation for the three models. When comparing results between LP and QCP, it is noticeable that the model based on quadratic programming outperforms the linear one, which makes the complete results much closer to the exact solution.

AC branch power flows are shown in Table VI. Average

Table IV
SUMMARY OF GENERATOR DATA BY GENERATOR TYPE

Code	Fuel	$P/\underline{P}$ [MW]	$Q/\underline{Q}$ [MVAr]	c [$/h]	a [$/MWh]	b $\left[\frac{\$/MW}{MWh}\right]$
$U12$	$\sharp 6Oil$	12/2.4	6/0	86.3852	56.5640	0.328412
$U20$	$\sharp 2Oil$	20/16	10/0	400.6849	130.0000	0.000000
$U50$	$Water$	50/10	16/-10	0.0010	0.0010	0.000000
$U76$	$Coal$	76/15.2	$30/-25$	212.3076	16.0811	0.014142
$U100$	$\sharp 6Oil$	100/25	60/0	781.5210	43.6615	0.052672
$U155$	$Coal$	155/54.3	$80/-50$	382.2391	12.3883	0.008342
$U197$	$\sharp 6Oil$	197/69	80/0	832.7575	48.5804	0.007170
$U350$	$Coal$	350/140	$150/-25$	665.1094	11.8495	0.004895
$U400$	U	400/100	$200/-50$	395.3749	4.4231	0.000213

Table V
ACTIVE POWER GENERATION LEVEL [MW] OF ALL UNITS

Bus No.	Unit	NLP	LP	QCP	Bus No.	Unit	NLP	LP	QCP
101	g_1	16	16	16	201	g_{33}	16	16	16
	g_2	16	16	16		g_{34}	16	16	16
	g_3	76	76	76		g_{35}	76	76	76
	g_4	76	76	76	202	g_{36}	16	16	16
102	g_5	16	16	16		g_{37}	16	16	16
	g_6	16	16	16		g_{38}	76	76	76
	g_7	76	76	76		g_{39}	76	76	76
	g_8	76	76	76	207	g_{40}	70.10	100	70.28
107	g_9	58.91	100	54.83		g_{41}	70.10	52.07	70.28
	g_{10}	58.91	40.04	54.83		g_{42}	70.10	100	70.28
113	g_{11}	69	69	69	213	g_{43}	83.96	69	79.16
	g_{12}	69	69	69		g_{44}	83.96	69	79.16
	g_{13}	69	69	69		g_{45}	83.96	69	79.16
114	g_{14}	0	0	0	214	g_{46}	0	0	0
115	g_{15}	2.4	2.4	2.4	215	g_{47}	2.4	2.4	2.4
	g_{16}	2.4	2.4	2.4		g_{48}	2.4	2.4	2.4
	g_{17}	2.4	2.4	2.4		g_{49}	2.4	2.4	2.4
	g_{18}	2.4	2.4	2.4		g_{50}	2.4	2.4	2.4
	g_{19}	2.4	2.4	2.4		g_{51}	2.4	2.4	2.4
	g_{20}	155	155	155		g_{52}	155	155	155
116	g_{21}	155	155	155	216	g_{53}	155	155	155
118	g_{22}	400	400	400	218	g_{54}	400	400	400
121	g_{23}	400	400	400	221	g_{55}	400	400	400
122	g_{24}	50	50	50	222	g_{56}	50	50	50
	g_{25}	50	50	50		g_{57}	50	50	50
	g_{26}	50	50	50		g_{58}	50	50	50
	g_{27}	50	50	50		g_{59}	50	50	50
	g_{28}	50	50	50		g_{60}	50	50	50
	g_{29}	50	50	50		g_{61}	50	50	50
123	g_{30}	155	155	155	223	g_{62}	155	155	155
	g_{31}	155	155	155		g_{63}	155	155	155
	g_{32}	350	350	350		g_{64}	-350	-350	-350
					302	g_{65}	200	200.2	220.53

Table VI
POWER FLOW [MW] OF AC BRANCHES

Branch	NLP	LP	QCP	Branch	NLP	LP	QCP
$P_{101-102}$	12.40	11.66	11.13	$P_{201-203}$	-12.61	-14.09	-12.83
$P_{101-103}$	-3.94	-5.32	-4.14	$P_{201-205}$	57.00	57.65	61.51
$P_{101-105}$	67.54	68.99	69.01	$P_{202-204}$	-7.60	-7.70	-14.84
$P_{102-104}$	45.15	43.07	43.22	$P_{202-206}$	50.14	49.75	53.09
$P_{102-106}$	54.25	54.44	54.91	$P_{203-209}$	19.38	17.20	18.09
$P_{103-109}$	30.72	29.20	26.93	$P_{203-224}$	-212.07	212.12	-211.01
$P_{103-124}$	-214.67	-215.33	-211.08	$P_{204-209}$	11.67	6.30	19.16
$P_{104-109}$	-29.54	-31.52	-31.43	$P_{205-210}$	-14.83	-13.82	-10.37
$P_{105-110}$	-4.57	-2.61	-3.09	$P_{206-210}$	-88.01	-87.46	-84.38
$P_{106-110}$	-84.11	-82.84	-82.66	$P_{207-208}$	86.31	125.75	85.85
$P_{107-108}$	88.17	109.93	87.34	$P_{208-209}$	-54.19	-37.53	-57.59
$P_{108-109}$	-48.43	-41.32	-52.06	$P_{208-210}$	-32.67	-9.57	-28.80
$P_{108-110}$	-35.67	-21.44	-32.88	$P_{209-211}$	-85.12	-80.35	-83.50
$P_{109-111}$	-98.84	-95.86	-103.97	$P_{209-212}$	-114.55	-109.52	-113.62
$P_{109-112}$	-125.05	-125.48	-129.39	$P_{210-211}$	-151.35	-138.97	-144.97
$P_{110-111}$	-147.33	-137.53	-144.88	$P_{210-212}$	-181.65	-168.14	-175.05
$P_{110-112}$	-174.44	-165.65	-170.28	$P_{211-213}$	-124.17	-105.38	-118.04
$P_{111-113}$	-129.94	-113.52	-144.05	$P_{211-214}$	-112.90	-115.17	-110.98
$P_{111-114}$	-116.88	-121.17	-105.43	$P_{212-213}$	-72.50	-55.09	-66.30
$P_{112-113}$	-83.67	-65.04	-100.44	$P_{212-223}$	-224.63	-226.74	-223.25
$P_{112-123}$	-216.76	-228.88	-200.15	$P_{213-223}$	-211.04	-222.25	-212.98
$P_{113-123}$	-196.34	-219.15	-168.61	$P_{214-216}$	-307.54	-312.06	-305.61
$P_{114-116}$	-311.55	-318.20	-300.00	$P_{215-216}$	64.62	67.39	75.56
$P_{115-116}$	72.03	69.98	74.24	$P_{215-221}$	-215.30	-218.45	-210.13
$P_{115-121}$	-220.35	-221.45	-219.73	$P_{215-224}$	215.97	218.45	215.15
$P_{115-124}$	218.67	217.68	215.22	$P_{216-217}$	-289.14	-300.00	-277.77
$P_{116-117}$	-312.81	-312.86	-312.68	$P_{216-219}$	96.56	106.20	97.83
$P_{116-119}$	123.48	115.23	137.21	$P_{217-218}$	-186.21	-181.96	-194.32
$P_{117-118}$	-177.29	-176.71	-177.42	$P_{217-222}$	-139.57	-140.28	-140.85
$P_{117-122}$	-138.23	-139.46	-138.26	$P_{218-221}$	-59.93	-57.79	-64.05
$P_{118-121}$	-55.44	-55.15	-55.53	$P_{219-220}$	-42.35	-37.66	-41.73
$P_{119-120}$	-28.97	-33.14	-22.18	$P_{220-223}$	-106.43	-102.03	-105.82
$P_{120-123}$	-93.01	-97.48	-86.20	$P_{221-222}$	-155.81	-157.09	-154.06
$P_{121-122}$	-157.16	-157.91	-156.68	$P_{301-302}$	-200.00	-200.20	-220.53
$P_{201-202}$	-44.39	-44.19	-48.68				

Table VII
POWER FLOW [MW] OF DC BRANCHES

Branch	NLP	LP	QCP
$P_{DC1-DC3}$	-97.31	-100	-104.20
$P_{DC2-DC3}$	-95.22	-91.88	-109.55
$P_{DC4-DC5}$	-34.12	-7.64	-69.01
$P_{DC4-DC6}$	-25.64	-8.98	-41.85
$P_{DC4-DC7}$	-18.40	-6.24	-25.02
$P_{DC5-DC7}$	13.59	0.00	37.49
$P_{DC6-DC7}$	-19.61	-7.43	-46.78

mismatches for LP and QCP are 5.68MW and 4.48MW, while the MAPEs are 8.42% and 7.72% respectively. Major discrepancies happen when there are high reactive power and low active power flowing on the corresponding circuit. *LP-OPF* model cannot approximate well in this case, i.e., when there is predominantly reactive power. In the case of the QCP model, the mismatch between the obtained solution and the exact one depends on the level of differences between real and reactive power, percentage of discrepancy varies. Table VII shows the DC branch power flows, while it can be seen that the *QCP-OPF* results are more accurate.

Generation levels are also better approximated with the quadratic version of the model. This fact can be explained because it maintains more intrinsic non-linearities of the problem which makes it a better solver for achieving closer-to-real solution. This can be seen from the comparisons of the objective function (O.F.) in Table VIII.

Last but not least, in order to assess the computational performance of the three models, Table VIII and IX show a comparison between solving one single system depicted in Fig. 4 and solving a virtual large system built via overlapping ten systems simultaneously. It first briefly compares the problem sizes, by indicating number of constraints, reflecting essentially the complexity of different formulation approaches. CPU time and number of iterations needed are shown subsequently. As a result, quadratic programming appears to be the most efficient one. When an exact problem is multiplied by ten times, computation time are merely increased by four times. LP underperforms a little bit, providing results 5.5 times slower. Although for NLP, computation time raises similar

amount, it is fundamentally way less efficient than other two models by two orders of magnitude. Therefore, when facing systems of thousands of nodes, presumably non-linear programming may not be applicable. Depending on the actual situation, either QCP or LP models presented in this paper could meet the requirements.

Table VIII
COMPUTATIONAL BURDEN COMPARISON (SINGLE SYSTEM)

Models	O.F. [$]	Constraints	CPU Time [s]	Variables
NLP	122492	789	11.481	969
QCP	121683	367	0.156	587
LP	117985	577	0.062	1210

Table IX
COMPUTATIONAL BURDEN COMPARISON (10 DUPLICATED SYSTEM)

Models	Constraints	CPU Time [s]	Variables
NLP	7881	48.017	9690
QCP	3661	0.733	5870
LP	5761	0.343	12100

VI. CONCLUSIONS

This paper presents two simplified models developed for solving OPF of a hybrid system based on VSC-MTDC. All network losses, as well as converter losses are considered. Moreover, different converter topologies can be taken into account by considering different converter parameters. Both models were verified by a full power flow solver to be general and compared using a MRTS network. Obtained results approximate the exact power flow solution well with a good level of accuracy, while maintaining non-linearity potentially results in greater computational burden. One possible application of these two models is to determine the preferred location/topology for MTDC networks. Another could be using approximated power flow solutions as starting point for the complete power flow solver, in order to accelerate the convergence. Moreover, both models can be extended to include security considerations. In future research, it can also serve as a *calculation module* for expansion planning where many different candidate lines can be considered.

ACKNOWLEDGMENT

This work has been carried out under the financial support of an European Project named BEST PATHS within the 7^{th} framework programme. The authors would like to thank the European Commission for the support.

REFERENCES

[1] D. Van Hertem and M. Ghandhari, "Multi-terminal vsc hvdc for the european supergrid: Obstacles," *Renewable and Sustainable Energy Reviews*, vol. 14, no. 9, pp. 3156–3163, December 2010. [Online]. Available: http://www.sciencedirect.com/science/article/pii/S1364032110002480

[2] "Wind in our sails. the coming of europe's offshore wind energy industry," 2011.

[3] "Roadmap to the supergrid technologies. update report," 2013.

[4] "Vsc transmission. working group b4.37," April.

[5] N. Flourentzou, V. Agelidis, and G. Demetriades, "Vsc-based hvdc power transmission systems: An overview," *Power Electronics, IEEE Transactions on*, vol. 24, no. 3, pp. 592–602, March 2009.

[6] J. Beerten, S. Cole, and R. Belmans, "Generalized steady-state vsc mtdc model for sequential ac/dc power flow algorithms," *Power Systems, IEEE Transactions on*, vol. 27, no. 2, pp. 821–829, May 2012.

[7] M. Baradar and M. Ghandhari, "A multi-option unified power flow approach for hybrid ac/dc grids incorporating multi-terminal vsc-hvdc," *Power Systems, IEEE Transactions on*, vol. 28, no. 3, pp. 2376–2383, Aug 2013.

[8] M. Baradar, M. Hesamzadeh, and M. Ghandhari, "Second-order cone programming for optimal power flow in vsc-type ac-dc grids," *Power Systems, IEEE Transactions on*, vol. 28, no. 4, pp. 4282–4291, Nov 2013.

[9] W. Feng, A. L. Tuan, L. Tjernberg, A. Mannikoff, and A. Bergman, "A new approach for benefit evaluation of multiterminal vsc-hvdc using a proposed mixed ac/dc optimal power flow," *Power Delivery, IEEE Transactions on*, vol. 29, no. 1, pp. 432–443, Feb 2014.

[10] A. Brooke, D. Kendrick, and A. Meeraus, *GAMS: A User's Guide*. Redwood City, California: The Scientific Press, 1992.

[11] P. Wong, P. Albrecht, R. Allan, R. Billinton, Q. Chen, C. Fong, S. Haddad, W. Li, R. Mukerji, D. Patton, A. Schneider, M. Shahidehpour, and C. Singh, "The ieee reliability test system-1996. a report prepared by the reliability test system task force of the application of probability methods subcommittee," *Power Systems, IEEE Transactions on*, vol. 14, no. 3, pp. 1010–1020, Aug 1999.

[12] J. Beerten, S. Cole, and R. Belmans, "A sequential ac/dc power flow algorithm for networks containing multi-terminal vsc hvdc systems," in *Power and Energy Society General Meeting, 2010 IEEE*, July 2010, pp. 1–7.

[13] "GAMS — The Solver Manuals," Oct. 2015. [Online]. Available: http://www.gams.com/help/topic/gams.doc/solvers/allsolvers.pdf

[14] P. Subcommittee, "IEEE Reliability Test System," *IEEE Transactions on Power Apparatus and Systems*, vol. PAS-98, no. 6, pp. 2047–2054, Nov. 1979.

[15] A. J. Wood and B. F. Wollenberg, *Power Generation, Operation, and Control*, 2nd ed. John Wiley & Sons, Nov. 2012.

[16] F. Desta Zahlay, L. Olmo, M. Rivier, F. de Cuadra, and J. I. PÃl'rez-Arriaga, "Finding a representative network losses model for large-scale transmission expansion planning with renewable energy sources," *Energy*, Dec. 2015. [Online]. Available: http://www.iit.upcomillas.es/publicaciones/mostrar_publicacion_revista.php.en?id=961

[17] A. Ramos and P. Sanchez-Martin, "Modeling Transmission Ohmic Losses in a Stochastic Bulk Production Cost Model," *Institute for Research in Technology, Madrid*, 1997. [Online]. Available: http://www.iit.upcomillas.es/~aramos/papers/losses.pdf

[18] J. Cao, W. Du, H. Wang, and S. Bu, "Minimization of Transmission Loss in Meshed AC/DC Grids With VSC-MTDC Networks," *IEEE Transactions on Power Systems*, vol. 28, no. 3, pp. 3047–3055, Aug. 2013.

[19] A. Gomez-Exposito, A. J. Conejo, and C. Canizares, *Electric Energy Systems: Analysis and Operation*, 1st ed. Boca Raton: CRC Press, Jul. 2008.

[20] P. K. M. Vormedal, "Voltage Source Converter Technology for Offshore Grids: Interconnection of Offshore Installations in a Multiterminal HVDC Grid using VSC," M. Sc. Thesis, 2010. [Online]. Available: http://brage.bibsys.no/xmlui/handle/11250/256956

[21] S. Cole, "Steady-state and dynamic modelling of VSC HVDC systems for power system Simulation," Ph.D. dissertation, PhD dissertation, Katholieke University Leuven, Belgium, 2010. [Online]. Available: http://www.esat.kuleuven.be/electa-projects/publications/fulltexts/pub_2143.pdf

[22] J. Zhu, *Optimization of power system operation*, 2nd ed. Piscataway, N.J.; Chichester: Wiley-IEEE ; John Wiley [distributor], 2015. [Online]. Available: http://search.ebscohost.com/login.aspx?direct=true&scope=site&db=nlebk&db=nlabk&AN=290214

Quanyu Zhao (S'12–M'14) is an assistant researcher at the Institute for Research in Technology (IIT). **Javier García - González** (S'99–M'01) is an Associate Professor at Universidad Pontificia Comillas, and belongs to the IIT.